Journal of Zhejiang University-SCIENCE A (Applied Physics & Engineering)
ISSN 1673-565X (Print); ISSN 1862-1775 (Online)
www.jzus.zju.edu.cn; www.springerlink.com
E-mail: jzus@zju.edu.cn

Analysis of pressure and flow compound control characteristics of an independent metering hydraulic system based on a two-level fuzzy controller*

Qi ZHONG[1], Bin ZHANG[†‡1], Hui-ming BAO[1], Hao-cen HONG[1], Ji-en MA[1], Yan REN[3], Hua-yong YANG[1], Rong-fong FUNG[2]

[1]*State Key Laboratory of Fluid Power and Mechatronic Systems, Zhejiang University, Hangzhou 310027, China*

[2]*Department of Mechanical and Automation Engineering, Kaohsiung First University of Science and Technology, Kaohsiung 000824, China*

[3]*College of Mechanical and Electrical Engineering, Wenzhou University, Wenzhou 325035, China*

[†]E-mail: zbzju@163.com

Received Sept. 3, 2018; Revision accepted Jan. 29, 2019; Crosschecked Feb. 14, 2019

Abstract: An independent metering valve control hydraulic system (IMVCHS) adopts two independent valves to separately control the meter-in and meter-out orifices. This structure increases the degree of freedom of the control, and improves its flexibility and energy-saving performance. In this study, an IMVCHS was established that applies a control system developed to research the pressure and flow compound control performance. A two-level fuzzy control algorithm based on the calculated flow rate feedback from the spool displacement was proposed to realize high precision flow control, and the two-level fuzzy control algorithm based on the pressure feedback was also adopted to enhance the pressure performance under a dynamic load. A simulation model was established, and its key parameters identified experimentally using the simulated load of a hydraulic bridge circuit. The experimental results show that the proposed flow controller has higher control accuracy with an error of less than 2%, and the flow adjustment time for 40 L/min step control is 320 ms. The pressure controller with a two-level closed-loop fuzzy algorithm can significantly improve these pressure dynamic and static performances, and achieve a step response time of less than 180 ms. Combining the pressure and flow controllers, the pressure and flow compound control of the IMVCHS is realized, and the capacity for coping with load fluctuations is also identified, with compound adjustment times of generally less than 200 ms, and occasionally less than 100 ms. This control system therefore achieves a good performance for pressure and flow compound control, and is able to widen the application of independent metering control technology.

Key words: Independent metering system; Pressure and flow compound control; Calculation flow rate feedback; Fuzzy proportion integral differential (PID); Two-level closed-loop control

https://doi.org/10.1631/jzus.A1800504 **CLC number:** TH137

1 Introduction

Owing to their high power-to-weight ratios, hydraulic systems are widely used in many different applications. In a typical operation, one actuator is controlled using a four-way directional valve. Using this type of valve, the meter-in and meter-out orifices are mechanically connected, and such coupling makes the actuator robust and easy to control, although it results in a lack of flexibility in the system (Eriksson and Palmberg, 2011; Zhang et al., 2018). In addition, the pressure and flow demands of an actuator vary significantly and frequently over time. Through a mechanical connection, either the pressure

‡ Corresponding author

* Project supported by the National Key Technology Support Program of China (No. 2014BAF02B00) and the National Science and Technology Major Project of China (No. 2012ZX04004021)

ORCID: Bin ZHANG, https://orcid.org/0000-0002-2290-9915

of the chamber or the flow through the orifice can be controlled, but not both. Therefore, unnecessary energy losses at a meter-out orifice and poor flexibility during an overrunning load will occur. This makes it difficult to optimize operating performance and energy-saving characteristics simultaneously. To overcome these shortcomings, Jansson and Palmberg (1990) adopted two valves to control the inlet and outlet orifices of the load individually. That innovation broke down the mechanical connection between the inlet and outlet orifices, increased the degree of freedom in the control, improved the flexibility of the actuator, and provided an effective method for saving energy in the hydraulic system as compared with a conventional directional valve-controlled hydraulic system. An independent metering valve control hydraulic system (IMVCHS) has particular functionalities that a traditional valve-controlled hydraulic systems cannot achieve, such as compound pressure and flow control, flow regeneration, and energy recovery.

Studies on IMVCHSs have been conducted for decades, and the major challenges in the design of such systems are the hardware layout and control strategy (Eriksson and Palmberg, 2011). Different IMVCHS layouts have been discussed by Sitte and Weber (2013). Eriksson (2007) designed an IMVCHS with four Valvistor valves. Liu and Yao (2002) and Yao and Liu (2002) achieved a good cylinder speed and system pressure using five proportional poppet valves, four of which are arranged for an independent metering function, and the last is used for flow regeneration. Linjama and Vilenius (2005) and Linjama et al. (2015) designed a digital flow control unit, which had a four-way valve configuration, with each path controlled independently using on/off valves connected in parallel. Eaton Co. (Yuan and Lew, 2005) developed a two-stage twin-spool servo valve for mobile applications. Yao et al. (2018) presented an independent metering pump control system, which used two pumps to individually control the meter-in and meter-out of a cylinder to achieve the performance of the IMVCHS.

Benefiting from the characteristics of independent metering control, an IMVCHS is more flexible in terms of the control and structure than a conventional valve-controlled system, and makes it easy to control both the chamber pressure and actuator speed (Borghi et al., 2014; Liu et al., 2017), reduce the vibrations of the actuator (Ding et al., 2017), and further realize energy-saving control (Choi et al., 2015; Liu et al., 2016; Ge et al., 2017). However, it also requires more complex control algorithms and more advanced hardware. In (Hu and Zhang, 2003), a conventional proportion integral differential (PID) controller was applied, upon which a fuzzy algorithm was added to an IMVCHS (Wei et al., 2016) and achieved a highly dynamic performance and significant potential for energy saving (Zhong et al., 2017). Hansen et al. (2011) studied the anti-load fluctuation performance of an IMVCHS using a dynamic pressure feedback algorithm. Ding et al. (2016) presented a bumpless mode switch controller for an IMVCHS to solve the problems of instability and roughness by using a discrete mode switch. A combined pump and valve control method was proposed to decouple the control for the actuator velocity and chamber pressure (Lantto et al., 1989; Xu et al., 2015). Owing to the strong nonlinearities and time-varying characteristics of a hydraulic system, adaptive control schemes were also applied to improve the control precision of an IMVCHS (Plummer and Vaughan, 1996; Book and Goering, 2001; Yao and DeBoer, 2002; Liu and Yao, 2008; Opdenbosch et al., 2011).

As mentioned above, existing studies on an IMVCHS have mainly focused on velocity control and energy-saving performance. Compound pressure and flow control is an effective method for dealing with both. However, the performance of both the flow and pressure controls is based on the position control characteristics of the valve, and those have generally been ignored in the reviewed studies because most of the valves used in the research have been mature industrial valves, equipped with matched displacement controllers. Therefore, it is difficult to study the influence of the valve motion on the performance of the pressure and flow controls.

To improve the performance of the compound pressure and flow controls for an IMVCHS, and thereby enhance the control precision of the actuator and optimize the energy-saving characteristics, a programmable control system is developed in this study to overcome the challenges in developing a hardware and control strategy. The system developed consists of spool displacement, and pressure and flow

controllers. A spool position controller based on a fuzzy PID (FPID) control algorithm is developed to improve the valve performance. A two-level fuzzy control algorithm based on the pressure feedback is proposed to improve the pressure dynamics, and reduce pressure fluctuations. A two-level closed-loop control strategy based on the calculated flow rate feedback from the spool displacement is also proposed to realize a highly precise flow control without the use of a transient flow meter or velocity sensor. To verify the effectiveness of the proposed controllers, an IMVCHS was designed, a simulation model was established, and a series of experiments on the pressure and flow control characteristics and compound control performance were carried out. The control system offers a better dynamic and robust performance, as well as the benefit of energy-saving operations.

The remainder of this paper is organized as follows. First, a brief introduction of an IMVCHS is given and relevant studies conducted in this area are provided. Then, the development of an IMVCHS is described and its mathematical model is analyzed. Furthermore, the development of a programmable control system for the IMVCHS is detailed. The developments of the FPID position control algorithm, the two-level fuzzy pressure control algorithm, and the two-level flow control algorithm based on the calculated flow rate feedback are also given. At last, a simulation model built for the developed IMVCHS is discussed along with experimental application of the developed control system, and the results are analyzed.

2 Hydraulic system configuration and modeling

The designed IMVCHS, shown in Fig. 1, is described in this section. The system is mainly made up of two two-stage proportional directional valves (2SPDVs) used for independent metering control, and a hydraulic bridge circuit with a proportional throttle valve used to simulate a dynamic load. To distinguish the two 2SPDVs in the following section, the pilot stage valve 4-1 and main stage valve 5-1 are defined as valve 1, and the pilot stage valve 4-2 and main stage valve 5-2 are defined as valve 2. The programmable controller receives the targets from the host computer, and feedback signals, including the displacement of the main spools, the pressure in the chambers, and the flow rate through the orifices, from the hydraulic system. Based on these signals, the controller outputs control signals to drive the two valves and achieve a fast response and high stability for both the pressure and flow in the IMVCHS. That is the main focus of the present study.

Three controllers are used in the control system, namely, the position controller, pressure controller, and flow controller. Thus, a mathematical analysis of the IMVCHS is divided into three aspects: valve dynamics, pressure dynamics, and flow dynamics.

2.1 Valve dynamics model

The actuator of the 2SPDV is a voice coil motor (VCM), which has a high acceleration and linear thrust. Its electrical characteristic in the moving coil can be written as

$$U = R_{\mathrm{c}} i + L_{\mathrm{c}} \frac{\mathrm{d}i}{\mathrm{d}t} + e_{\mathrm{b}}, \tag{1}$$

where U is the driving voltage, R_{c} is the equivalent resistance, L_{c} is the equivalent inductance, i is the current in the coil, t is the time, and e_{b} is the back electromotive force, which can be determined as

$$e_{\mathrm{b}} = BLv, \tag{2}$$

where B is the magnetic induction intensity of the VCM, L is the total length of the coil, and v is the velocity of the moving coil. The electromagnetic force of the VCM can be expressed as

$$F_{\mathrm{c}} = BiL. \tag{3}$$

Because the current amplifier has a much faster dynamic performance than the pilot spool position, the current characteristic can be neglected in the mathematic model of the valve motion to reduce the system order. It is assumed that the pilot spools are critically centered and subjected to the VCM output force, reset spring force, damping force, and flow

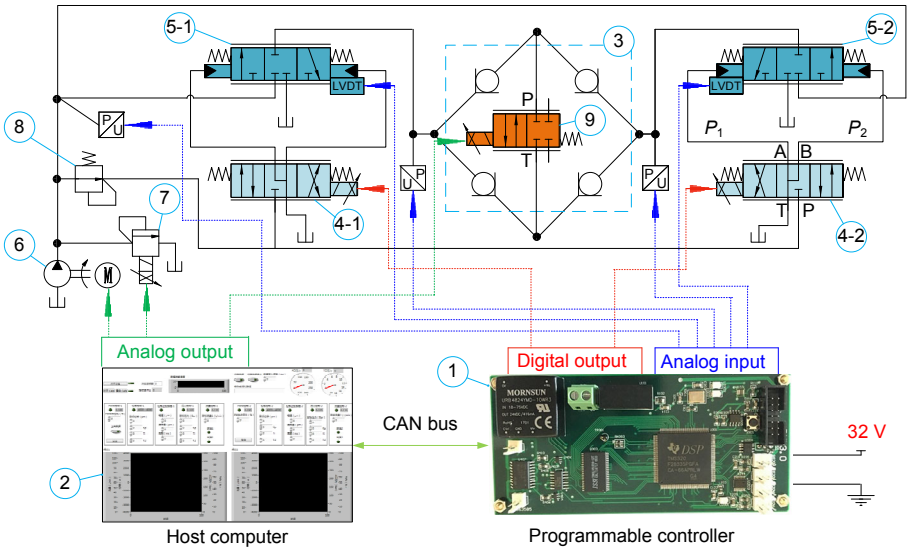

Fig. 1 Structure of the IMVCHS

1: programmable controller; 2: host computer; 3: hydraulic bridge circuit; 4: pilot stage valve; 5: main stage valve; 6: fixed displacement pump; 7: relief valve; 8: pressure reducing valve; 9: proportional throttle valve. LVDT: linear variable differential transformer; CAN: controller area network

force. The state-space model of the pilot stage valve is given as a canonical controllable form:

$$\begin{aligned}
&\dot{\boldsymbol{x}}=\boldsymbol{A}\boldsymbol{x}+\boldsymbol{B}u+\boldsymbol{M}F_{\mathrm{f1}},\\
&y=x_1,\\
&\boldsymbol{x}=\begin{bmatrix}x_1\\ \dot{x}_1\end{bmatrix},\quad u=U,\\
&\boldsymbol{A}=\begin{bmatrix}0 & 1\\ -\dfrac{k_{\mathrm{e1}}}{m_1} & -\dfrac{k_{\mathrm{d1}}}{m_1}\end{bmatrix},\\
&\boldsymbol{B}=\begin{bmatrix}0\\ \dfrac{c_{\mathrm{i}}BL}{m_1}\end{bmatrix},\quad \boldsymbol{M}=\begin{bmatrix}0\\ \dfrac{-1}{m_1}\end{bmatrix},
\end{aligned}\tag{4}$$

where x_1 is the displacement of the pilot spool, m_1 is the moving mass of the pilot stage, k_{e1} is the equivalent elastic load coefficient of the pilot stage, k_{d1} is the equivalent damping coefficient in the pilot stage, c_{i} is the linear equivalent gain of the current amplifier, and F_{f1} is the total flow force exerted on the pilot spool.

The 2SPDV is a two-stage valve, where the main spool is driven based on the differential pressure of the main valve control chambers. Therefore, the main spool is subject to the control pressure force, compression spring force, viscous force, and flow force. The state-space model of the main stage valve is expressed as follows:

$$\begin{aligned}
&\dot{\boldsymbol{x}}=\boldsymbol{A}_{\mathrm{m}}\boldsymbol{x}+\boldsymbol{B}_{\mathrm{m}}u+\boldsymbol{M}_{\mathrm{m}}F_{\mathrm{f2}},\\
&y=x_2,\\
&\boldsymbol{x}=\begin{bmatrix}x_2\\ \dot{x}_2\end{bmatrix},\quad u=P_1-P_2,\\
&\boldsymbol{A}_{\mathrm{m}}=\begin{bmatrix}0 & 1\\ -\dfrac{k_{\mathrm{e2}}}{m_2} & -\dfrac{k_{\mathrm{d2}}}{m_2}\end{bmatrix},\\
&\boldsymbol{B}_{\mathrm{m}}=\begin{bmatrix}0\\ \dfrac{S}{m_2}\end{bmatrix},\quad \boldsymbol{M}_{\mathrm{m}}=\begin{bmatrix}0\\ \dfrac{-1}{m_2}\end{bmatrix},
\end{aligned}\tag{5}$$

where x_2 is the displacement of the main spool, m_2 is the moving mass of the main stage, k_{e2} is the equivalent elastic load coefficient of the main stage, k_{d2} is the equivalent damping coefficient in the main stage, P_1 and P_2 are the pressures in the left and right control chambers of the main stage valve, respectively, S is the equivalent cross area of the main valve control chamber, and F_{f2} is the flow force exerted on the main spool.

The flow force applied to a spool is given as

$$F_{fi}=-F_{si}-F_{ti},\tag{6}$$

where the subscript i (i=1, 2) represents the number of stages of the pilot stage valve and main stage valve; F_{s1} and F_{s2} are the steady flow forces acting on the pilot spool and main spool, respectively; F_{t1} and F_{t2} are the transient flow forces applied to the pilot spool and main spool, respectively.

The steady flow force in the valve is caused by the changes in momentum. This type of force tends to close the orifices and can be presented as

$$F_{si}=2W_iC_dC_v\cos(\theta)\Delta P_ix_i, \tag{7}$$

and the transient flow force is given as

$$F_{ti}=W_iC_dl_i\sqrt{2\rho\Delta P_i}\dot{x}_i, \tag{8}$$

where W_i is the area gradient, C_d is the flow coefficient, C_v is the fluid velocity coefficient, θ is the flow angle, ΔP_i is the pressure drop across the valve orifice, l_i is the total damping length of the fluid in the valve, and ρ represents the density of the oil.

2.2 Flow dynamics model

The flow rate through a valve orifice is calculated by

$$Q_i=C_dA_i\sqrt{\frac{2\Delta P_i}{\rho}}, \tag{9}$$

where A_i is the orifice area.

For the pilot stage, the differential pressure through the orifice is detailed as follows:

$$\Delta P_{1L}=\begin{cases}P_p-P_1, & x_1\geq 0,\\ P_1-P_t, & x_1<0,\end{cases} \tag{10a}$$

$$\Delta P_{1R}=\begin{cases}P_2-P_t, & x_1\geq 0,\\ P_p-P_2, & x_1<0,\end{cases} \tag{10b}$$

where P_p is the supply pressure for the pilot valve, P_t is the pressure of the oil tank, ΔP_{1L} is the pressure difference between the pilot port P(T) and pilot operation port A that connects to the left control chamber of the main stage valve, and ΔP_{1R} is the pressure difference between the pilot port P(T) and pilot operation port B that connects to the right control chamber of main stage valve, as shown in Fig. 1.

Because the main stage valve has a three-position and three-way structure, the pressure difference through the main valve orifice is given as

$$\Delta P_2=\begin{cases}P_s-P_A, & x_2<0,\\ P_B-P_t, & x_2\geq 0,\end{cases} \tag{11}$$

where P_s is the supply pressure for the IMVCHS, P_A is the pressure of the chamber connecting to port P of the proportional throttle valve in the hydraulic bridge circuit, and P_B is the pressure of the chamber connecting to port T of the proportional throttle valve, as shown in Fig. 1.

2.3 Pressure dynamics model

The main valve response is influenced by the pressure changes of the control chambers. To determine the chamber pressure, the basic fluid continuity equations are given as

$$\begin{aligned}\dot{P}_1&=\operatorname{sign}(\dot{x}_2)\frac{\beta}{V_L}\left(C_dA_1\sqrt{\frac{2\Delta P_{1L}}{\rho}}-S\dot{x}_2\right),\\ \dot{P}_2&=\operatorname{sign}(\dot{x}_2)\frac{\beta}{V_R}\left(S\dot{x}_2-C_dA_1\sqrt{\frac{2\Delta P_{1R}}{\rho}}\right),\end{aligned} \tag{12}$$

where V_L and V_R are the volumes of the left and right control chambers of the main stage valve, respectively, and β is the oil bulk modulus.

Similarly, the pressure dynamics in the hydraulic bridge circuit is expressed as follows:

$$\begin{aligned}\dot{P}_P&=\frac{\beta}{V_P}\left(C_dA_2\sqrt{\frac{2\Delta P_2}{\rho}}-Q_{PT}\right),\\ \dot{P}_T&=\frac{\beta}{V_T}\left(Q_{PT}-C_dA_2\sqrt{\frac{2\Delta P_2}{\rho}}\right),\end{aligned} \tag{13}$$

where V_P and V_T are the volumes of the chambers that connect to ports P and T of the proportional throttle valve, respectively, P_P and P_T are the pressures in the two chambers, respectively, and Q_{PT} is the flow through the throttle valve. The selection of a positive

or negative sign is determined based on the flow direction of the fluid.

3 Control system design

The structure of the control system is shown in Fig. 2. It consists of three loops, namely, displacement, pressure, and flow loops. The controller receives both the target and feedback signals including the displacement of the main spools, pressures of the actuator chambers, and the flow rate through the orifices. Based on these signals, the controller drives the two valves to achieve a fast response and high stability of both the pressure and flow in the IMVCHS. That is the main focus of this study.

Differing from a traditional valve control system, the controller in the IMVCHS needs to drive two valves synchronously and switch over multiple control modes. Therefore, the IMVCHS control system requires stronger hardware and a more advanced algorithm. According to this control structure, a programmable control system including the host and lower controllers is developed in this study, as shown in Figs. 3 and 4.

The host controller provides a friendly user interface and communicates with the lower controller through the CAN bus, and monitors the state of the IMVCHS. The controller was designed based on a minimum float-point digital signal processor (DSP) system, and a Texas Instruments-Real Time Operating System (TI-RTOS) embedded operating system was adopted to realize a parallel-thread operation with a closed-loop control frequency of 0.5 ms. Expanded using a power management module, a signal processing module, a CAN communication module, and a digital drive module of the VCM, the controller can realize a high-speed data acquisition, an accurate data transmission, and a precision digital control.

The implementation of the driving module is illustrated in Fig. 5, which is an H bridge circuit. The carrier frequency of the pulse width modulation (PWM) is set to 10 kHz and the power source is 32 V. To avoid a short pass in the H bridge circuit, a signal inverter module is applied to reverse the digital signal from the DSP, and thus the H bridge circuit receives two adverse PWM signals, and the metal-oxide-semiconductor field-effect transistor (MOSFET) on the same side cannot be opened at the same time. The duty ratio of the PWM determines the direction and values of the VCM output force. The effective driving voltage can be expressed as

$$U=(2\mu-1)U_{\mathrm{s}}, \tag{14}$$

where μ is the duty ratio of the PWM, and U_{s} is the supply voltage of the driving circuit.

3.1 Position controller

Most of the proportional valves used in the IMVCHS are industrial valves, and have their own matched position controllers, and thus studies on an IMVCHS have usually focused on system performance, while ignoring the valve characteristics. However, as illustrated in Fig. 2, the position loop is

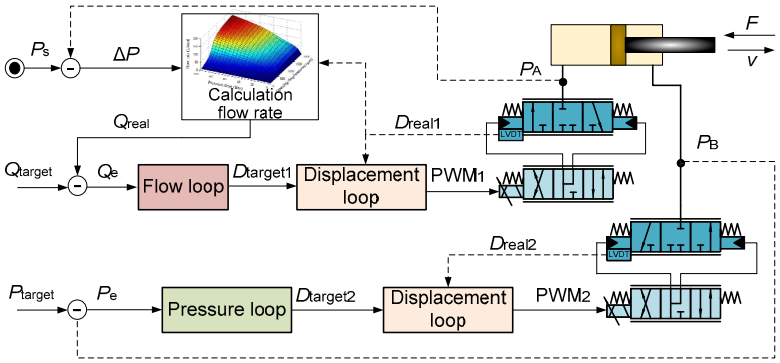

Fig. 2 Pressure and flow compound control structure of IMVCHS

P_{e}: pressure error; Q_{e}: flow rate error; Q_{real}: real flow rate; Q_{target}: target flow rate; D_{target1}: target displacement of valve 1; D_{target2}: target displacement of valve 2; D_{real1}: real displacement of valve 1; D_{real2}: real displacement of valve 2

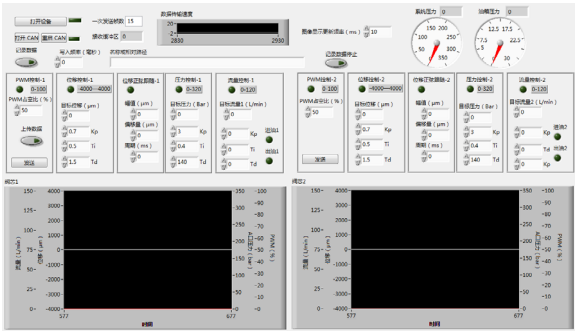

Fig. 3 Interface of host controller

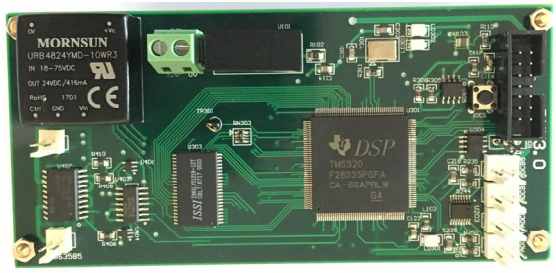

Fig. 4 Programmable lower controller

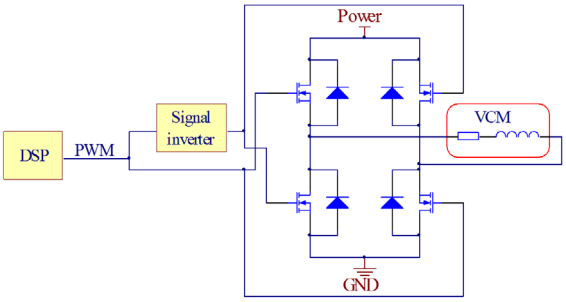

Fig. 5 Block diagram of VCM driving circuit

the inner loop of both the pressure and flow loops, and thus the valve position performance will directly affect the performance of the pressure and flow controls. The design of a high-performance valve position controller is an effective method for improving the pressure and flow control performance.

A current loop is usually used in certain advanced direct-drive valve controllers (Wu et al., 2014; Acuña-Bravo et al., 2017). However, in a 2SPDV, the main spool position is disproportional to the driving current. Therefore, the current loop gives little help towards improving the spool position control performance, and only a displacement loop is applied in the position controller. The classic PID control algorithm cannot meet the existing contradiction between stability and rapidity in a fast-response 2SPDV. Therefore, a FPID control algorithm is applied in the displacement loop, as shown in Fig. 6.

The formula of the position FPID control algorithm is expressed in Eq. (15).

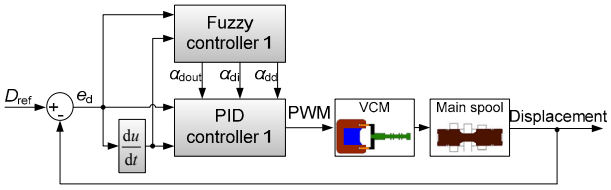

Fig. 6 Spool position control structure
D_{ref} is the displacement reference

$$U(k)=\alpha_{dout}\left\{k_p e_d(k)+k_i\sum_{i=0}^{k}[\alpha_{di}e_d(i)] +\alpha_{dd}k_d[e_d(k)-e_d(k-1)]\right\}, \tag{15}$$

where $e_d(k)$ is the displacement error, k_p, k_i, and k_d are the parameters of the PID controller, and α_{dout}, α_{di}, and α_{dd} are the outputs of the displacement fuzzy controller. The on-line optimization of α_{dout} is a compromise between the dynamics and stability of the valve motion. In addition, the choice of α_{di} incurs a conflict between the control accuracy and stability of the valve. Similarly, the changing process of α_{dd} is a balance between the response speed and an overshoot. As a rule in determining the key parameters of the FPID controller, the spool obtains high control accuracy with an acceptable dynamic performance of the position control, but without an overshoot. Because the pressure of the chamber is extremely sensitive when the main spool is close to the critical closing position, a slight overshoot of the main spool will cause significant fluctuations of the chamber pressure. According to Eq. (5), the dynamics of the main spool are determined based on the spool displacement, spool velocity, and many other factors. Therefore, with this position fuzzy controller, both $e_d(k)$ and $\Delta e_d(k)$, which can be equivalent to spool displacement x_2 and spool velocity $\dot{x}_2$, respectively, are considered as variable inputs, as shown in Fig. 7.

In the scale transform of the fuzzifier, a linear transformation method is applied, which is as follows:

$$E=\frac{E_{\max}-E_{\min}}{e_{\max}-e_{\min}}\left(e-\frac{e_{\max}+e_{\min}}{2}\right)+\frac{E_{\max}+E_{\min}}{2},$$
$$\Delta E=\frac{\Delta E_{\max}-\Delta E_{\min}}{\Delta e_{\max}-\Delta e_{\min}}\left(\Delta e-\frac{\Delta e_{\max}+\Delta e_{\min}}{2}\right)+\frac{E\Delta_{\max}+\Delta E_{\min}}{2}, \quad (16)$$

where e is the control error, Δe is the change rate of the control error, $e_{\min}$ and $e_{\max}$ are the minimum and maximum values of the control error, respectively, E is the control error after scale transform, ΔE is the change rate of the control error after scale transform, and $E_{\min}$ and $E_{\max}$ are the minimum and maximum control errors after scale transform, respectively.

During the fuzzy process, $[E_{\min}, E_{\max}]$ and $[\Delta E_{\min}, \Delta E_{\max}]$ are defined within the same range of $[-1, 1]$. The membership functions are as illustrated in Fig. 8, where NB, NM, NS, Z, PS, PM, and PB represent largely negative, moderately negative, slightly negative, neutral, slightly positive, moderately positive, and largely positive, respectively.

Fuzzy rules determine the on-line optimization results of α_{dout}, α_{di}, and α_{dd}, which are the key parameters of the FPID controller used to solve the contradiction between the stability and dynamics in a 2SPDV. The rule base of a position fuzzy controller is shown in Table 1, where M, B, S, VB, and VS indicate moderate, large, small, extremely large, and extremely small, respectively.

The output rule is expressed as follows:

$$R^i:\ \text{if}\ e_{\text{d}}(k)=A_1^i,\ \text{and}\ \Delta e_{\text{d}}(k)=A_2^i,\ \text{then}\ \boldsymbol{Y}=\boldsymbol{E}_i, \quad (17)$$

where R^i is the ith fuzzy rule, A_1^i and A_2^i are the variable inputs, $\boldsymbol{Y}$ is the result of the fuzzy rule, and $\boldsymbol{E}_i=[E_1, E_2, E_3]^{\text{T}}$ is the output of the ith fuzzy rule. Using the product inference engine, a singleton fuzzifier, and a center-average defuzzifier, the output of the fuzzy system can be given as

$$[\alpha_{\text{DOUT}}, \alpha_{\text{DI}}, \alpha_{\text{DD}}]^{\text{T}}=\frac{\sum_{i=1}^{p}\left[\mu_{A_1^i}(e_{\text{d}})\mu_{A_2^i}(\Delta e_{\text{d}})\right]\boldsymbol{E}_i}{\sum_{i=1}^{p}\left[\mu_{A_1^i}(e_{\text{d}})\mu_{A_2^i}(\Delta e_{\text{d}})\right]}, \quad (18)$$

where α_{DOUT}, α_{DI}, and α_{DD} are the outputs of the defuzzy process of the displacement fuzzy controller, $\mu_{A_1^i}(e_{\text{d}})$ and $\mu_{A_2^i}(\Delta e_{\text{d}})$ are the membership function

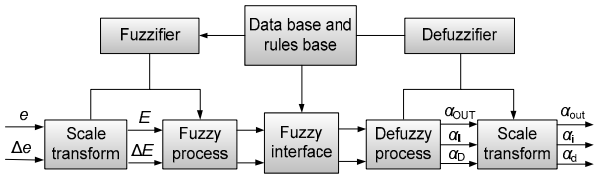

Fig. 7 Structure of fuzzy controller

α_{OUT}, α_{I}, and α_{D} are the outputs of the defuzzy process; α_{out}, α_{i}, and α_{d} are the outputs of the fuzzy controller

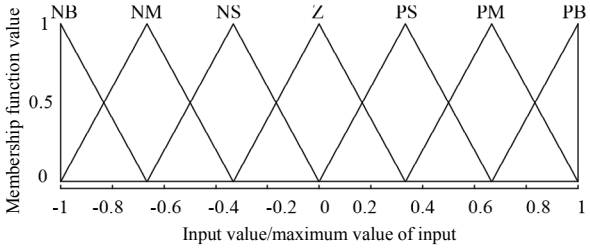

Fig. 8 Membership functions of the inputs

Table 1 Rule base of position fuzzy controller

α_{DOUT}, α_{DI}, α_{DD}		$e_{\text{d}}(k)$						
		NB	NM	NS	Z	PS	PM	PB
$\Delta e_{\text{d}}(k)$	NB	M, Z, Z	VB, S, Z	VB, VB, VB	B, VB, VB	B, M, B	M, Z, Z	S, Z, Z
	NM	M, Z, Z	B, VS, Z	B, VB, M	M, VB, B	M, M, M	M, Z, Z	S, Z, Z
	NS	S, Z, Z	M, VS, Z	M, B, M	S, B, M	M, B, S	M, Z, Z	S, Z, Z
	Z	S, Z, Z	M, Z, Z	M, B, Z	Z, M, Z	M, B, Z	M, Z, Z	S, Z, Z
	PS	S, Z, Z	M, Z, Z	M, B, S	S, B, M	M, B, M	M, VS, Z	S, Z, Z
	PM	S, Z, Z	M, Z, Z	M, M, M	M, VB, B	B, VB, B	B, VS, Z	M, Z, Z
	PB	S, Z, Z	M, Z, Z	B, M, B	B, VB, VB	VB, VB, VB	VB, S, Z	M, Z, Z

values of $e_d(k)$ and $\Delta e_d(k)$, respectively, and p is the number of fuzzy rules.

During the defuzzy process, the membership functions of the three outputs are as shown in Fig. 9.

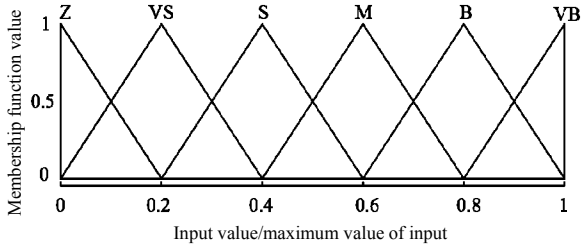

Fig. 9 Membership functions of the outputs

The scale transform of the fuzzifier is given as

$$\begin{cases} \alpha_{\text{dout}} = k_1 \alpha_{\text{DOUT}}, \\ \alpha_{\text{di}} = k_2 \alpha_{\text{DI}}, \\ \alpha_{\text{dd}} = k_3 \alpha_{\text{DD}}, \end{cases} \tag{19}$$

where k_1, k_2, and k_3 are the output scaling factors of the fuzzy controller.

3.2 Pressure controller

The pressures of the meter-in and meter-out are coupled through the load. Pressure vibrations on one side will cause corresponding pressure vibrations on the other side. To dampen the oscillations of the chamber pressure, a two-level fuzzy control algorithm is developed to improve the pressure dynamics and stability. The outer loop is a pressure loop, the results of which are the target references of the inner displacement loop. This is illustrated in Fig. 10. The scale transforms, membership functions, and defuzzy rules in the pressure fuzzy controller have the same form as the position fuzzy controller, which is illustrated in Eqs. (16)–(19) and Figs. 8 and 9.

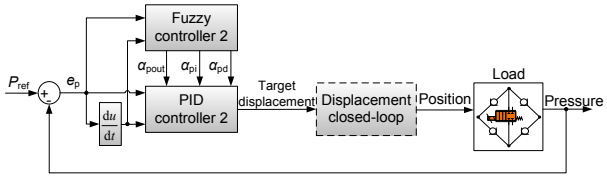

Fig. 10 Chamber pressure control structure
P_{ref} is the pressure reference

The formula of the pressure FPID control algorithm is given as

$$\begin{aligned} \Delta x(k) = \alpha_{\text{pout}} \Bigg\{ & k_{\text{p}} e_{\text{p}}(k) + k_{\text{i}} \sum_{i=0}^{k} [\alpha_{\text{pi}} e_{\text{p}}(i)] \\ & + \alpha_{\text{pd}} k_{\text{d}} [e_{\text{p}}(k) - e_{\text{p}}(k-1)] \Bigg\}, \end{aligned} \tag{20}$$

where $e_p(k)$ is the pressure error, $\Delta x(k)$ is the spool position increment, and α_{pout}, α_{pi}, and α_{pd} are the outputs of the pressure fuzzy controller. For the displacement, a positive value is defined as the operation port being connected with the tank, and a negative value as the operation port being connected with the supply pressure, as illustrated in Eq. (11). Thus, the reference displacement is expressed as

$$x(k)_{\text{ref}} = x(k)_{\text{rel}} - \Delta x(k), \tag{21}$$

where $x(k)_{\text{rel}}$ is the current spool position, and $x(k)_{\text{ref}}$ is the target displacement of the inner displacement loop. The pressure pulsation of the pump, the dynamic load, and many other factors will result in an oscillation of the chamber pressure, and cause instability in the pressure controller. To avoid such phenomena, an average filter is applied, which is expressed as

$$P(k) = \frac{\sum_{k=1}^{k=n} P(k-n+1)}{n}, \tag{22}$$

where $P(k)$ is the chamber pressure of the load and is a compromise between the dynamics and accuracy of the chamber pressure, and n is a constant. The fuzzy rules of the pressure fuzzy controller are detailed in Table 2.

3.3 Flow controller

A closed-loop flow control using flow sensors has been excluded because it is too expensive for practical use (Sitte et al., 2014). In some specific loads, such as a cylinder or hydraulic motor, the flow through a valve can be measured based on the cylinder velocity or motor speed. However, this requires an additional sensor and cannot adapt all types of loads because it cannot be directly measured to calculate the

flow. In (Liu and Yao, 2008) and (Xu et al., 2015), a calculation flow rate feedback control algorithm was presented; in addition, the control voltage was equivalent to the spool displacement, and was used as the input of the calculation flow rate algorithm. Although a time delay and errors occur between the control voltage signal and the corresponding spool displacement, dynamic and static errors in the valve are typically ignored in a system analysis. Therefore, the previous method (Liu and Yao, 2008; Xu et al., 2015) will affect the accuracy and dynamic performance of a flow closed-loop control. Considering the effects from the valve dynamics, this study employs a calculation flow rate feedback control algorithm based on the pressure and spool displacement feedback to realize an indirect measurement of the flow rate. The flow mapping of the tested 2SPDV is shown in Fig. 11.

A two-level controller is also applied in the flow rate closed-loop control algorithm by means of valve flow mapping, as shown in Fig. 12. Similarly, the flow fuzzy controller has the same rules as the displacement fuzzy controller, including scale transforms, membership functions, and defuzzy rules. The rule base of the flow fuzzy controller is shown in Table 3.

The expression of the flow FPID controller is given in Eq. (23).

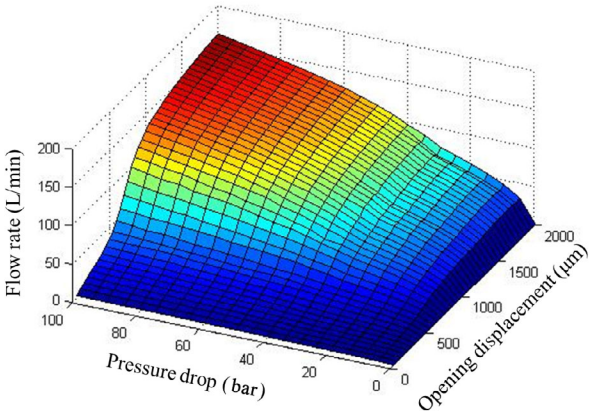

Fig. 11 Flow mapping of experimental valve (1 bar= 0.1 MPa)

Table 2 Rule base of pressure fuzzy controller

α_{POUT}, α_{PI}, α_{PD}		$e_p(k)$						
		NB	NM	NS	Z	PS	PM	PB
$\Delta e_p(k)$	NB	M, Z, Z	B, M, Z	VB, VB, VB	S, B, Z	B, M, VB	M, Z, Z	S, Z, Z
	NM	M, Z, Z	B, S, Z	VB, VB, B	VS, B, Z	B, B, B	M, Z, Z	M, Z, Z
	NS	M, Z, Z	B, VS, Z	B, B, B	Z, Z, Z	B, B, B	M, Z, Z	M, Z, Z
	Z	M, Z, Z	B, VS, Z	B, B, M	Z, Z, Z	B, B, M	B, VS, Z	M, Z, Z
	PS	M, Z, Z	M, Z, Z	B, B, B	Z, Z, Z	B, B, B	B, VS, Z	M, Z, Z
	PM	M, Z, Z	M, Z, Z	B, B, B	VS, B, Z	VB, VB, B	B, S, Z	M, Z, Z
	PB	S, Z, Z	M, Z, Z	B, M, VB	S, B, Z	VB, VB, VB	B, M, Z	M, Z, Z

α_{POUT}, α_{PI}, and α_{PD} are the outputs of the defuzzy process of the pressure fuzzy controller

Table 3 Rule base of flow fuzzy controller

α_{QOUT}, α_{QI}, α_{QD}		$e_q(k)$						
		NB	NM	NS	Z	PS	PM	PB
$\Delta e_q(k)$	NB	B, Z, Z	M, S, Z	VB, VB, B	B, M, Z	M, S, B	S, Z, Z	M, Z, Z
	NM	B, Z, Z	M, VS, Z	B, VB, B	M, M, Z	B, M, M	M, Z, Z	B, Z, Z
	NS	B, Z, Z	M, VS, Z	B, B, M	S, S, Z	B, B, S	M, Z, Z	B, Z, Z
	Z	B, Z, Z	M, VS, Z	B, B, VS	S, Z, Z	B, B, VS	M, VS, Z	B, Z, Z
	PS	B, Z, Z	M, Z, Z	B, B, S	S, S, Z	B, B, M	M, VS, Z	B, Z, Z
	PM	B, Z, Z	M, Z, Z	B, M, M	M, M, Z	B, VB, B	M, VS, Z	B, Z, Z
	PB	M, Z, Z	S, Z, Z	M, S, B	B, M, Z	VB, VB, B	M, S, Z	B, Z, Z

α_{QOUT}, α_{QI}, and α_{QD} are the outputs of the defuzzy process of the flow fuzzy controller

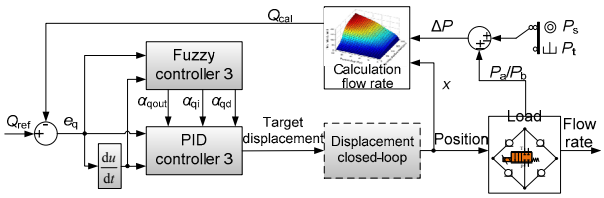

Fig. 12 Flow rate control structure

Q_{ref}: flow rate reference; Q_{cal}: calculation flow rate; ΔP: differential pressure

$$\Delta x(k)=\alpha_{qout}\left\{k_p e_q(k)+k_i\sum_{i=0}^{k}[\alpha_{qi}e_q(i)]+\alpha_{qd}k_d[e_q(k)-e_q(k-1)]\right\},\quad(23)$$

$$x(k)_{ref}=x(k)_{rel}+\mathrm{sign}[x(k)_{rel}]\Delta x(k),$$

where $e_q(k)$ is the flow rate error, and α_{qout}, α_{qi}, and α_{qd} are the outputs of the flow fuzzy controller.

The better the flow dynamics are, more easily a fast spool motion and pressure vibrations occur. Thus, the fuzzy rules of the flow fuzzy controller can be determined using a conservative approach to avoid a flow overshoot and pressure impact. As the calculation input of the flow rate feedback control algorithm, a violent change in pressure will eventually affect the flow rate, and result in system instability.

4 Simulation and experiment analysis

The differences in performance of both a conventional PID controller and the FPID controller were compared through simulations conducted on the MATLAB/AMESim co-simulation platform. The simulation model was established according to the structure of the designed IMVCHS, as shown in Fig. 1. A hydraulic bridge circuit with a proportional throttle valve was adopted for the dynamic load. The AMESim software was used to model the hydraulic unit, whereas MATLAB was used to model the proposed controller. Based on practical measurements, some key parameters of the IMVCHS were obtained during the simulations, as shown in Table 4.

4.1 Experimental test on positional control

As an inner controller, the position controller is the basis for realizing the pressure and flow controls. Thus, a good control performance will significantly help with the pressure and flow controls.

Table 4 Structural parameters of IMVCHS

Parameter	Value
Resistance of VCM coil (Ω)	55.6
Coil turns of VCM	272
Moving mass of pilot stage (g)	11.7
Diameter of the pilot spool (mm)	8
Reset spring coefficient of pilot stage (N/mm)	16.7
Supply pressure of pilot stage (MPa)	2
Supply voltage of VCM (V)	32
Moving mass of main stage (g)	75.5
Diameter of the main spool (mm)	16
Overlap of main stage (mm)	1
Pre-pressing force of main stage (N)	16
Reset spring coefficient of main stage (N/mm)	8

The displacement control performances for both the simulations and experiments are given in Fig. 13. The parameters of the position FPID controller were optimized during the simulations, and were determined as follows: k_p=1.5, k_i=8.0, and k_d=0.002. Fig. 13a shows that the position step response of a classical PID controller has a longer adjustment time of 400 ms, and a larger overshoot of 25%. In contrast, the FPID controller has a very short adjustment time and almost no overshoot. It can be seen that the adjustment time is only 40 ms for a 50% full stroke. A step response experiment was also conducted to verify the simulation model, and k_p, k_i, and k_d were set to 1.4, 10.0, and 0.004, respectively. As shown in Fig. 13b, the performance of the valve is well matched with the simulation results, verifying the correctness of the simulation model.

The frequency response is also evaluated using sinusoidal signal tracking experiments. It is known that the classical PID algorithm cannot track the sinusoidal reference effectively, and will thus create instability in the system. Therefore, the experimental results only include the FPID controller, and the 5-Hz and 10-Hz position sinusoidal signal responses of the tested 2SPDV are as illustrated in Fig. 14. When tracking a 5-Hz sinusoidal signal of 0.2 mm in amplitude, the spool is easily able to catch the target, and a slight overshoot occurs when the command

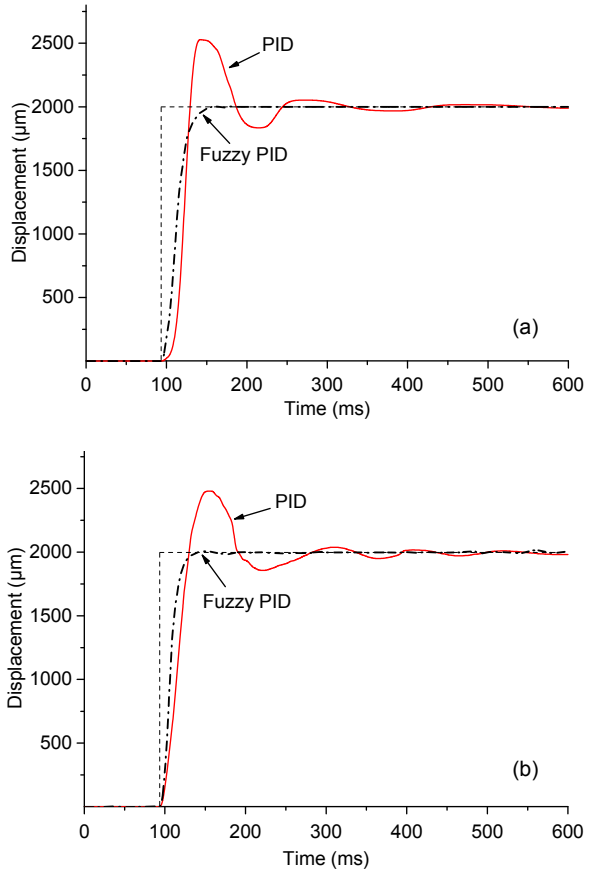

Fig. 13 Position step response: (a) simulation result; (b) experiment result

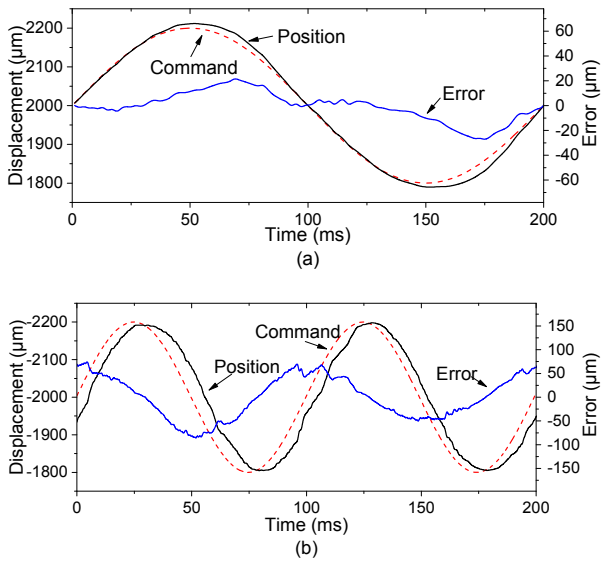

Fig. 14 Position frequency response: (a) 5 Hz; (b) 10 Hz

sinusoidal signal is close to the extreme value, and the error can be controlled to within 20 μm. When the signal frequency is increased to 10 Hz, the spool maintains almost the same amplitude as the commands, but an average delay time of 5 ms occurs. These results indicate that the proposed position FPID controller can solve well the contradiction between the rapidity and stability, and still meet the requirements of the IMVCHS.

Because both the pressure and flow controllers are two-level closed-loop controllers, the hysteresis and overshoot of one closed-loop will eventually accumulate in the other loop, and cause the system to lose control. Therefore, all comparisons of the pressure and flow controls are carried out using the FPID algorithm.

4.2 Experimental test on pressure control

To improve energy-saving performance, the valve controlling the meter-out should be fully opened to decrease the backpressure. However, the issues of controllability and stability of the actuator also need to be taken into account. Hence, the backpressure should have a fast dynamic characteristic to increase the response speed of the dynamic damping of the actuator and further improve its motion performance. The backpressure is controlled using valve 2, and the experiments are carried out under a 60-L/min output flow rate of the pump. The parameters of the pressure FPID controller are set at: k_p=3.0, k_i=7.5, and k_d=42.0. Using 5, 30, and 60 bar as references, the pressure of outlet chamber is given in Fig. 15a. The adjustment time of the pressure step from 5 to 30 bar is approximately 290 ms, and the overshoot can be controlled at under 8%. When increasing the pressure from 30 to 60 bar, the adjustment time is reduced to 180 ms, and the overshoot is optimized to within 6%, which is due to the approximately 90 μm distance between the target spool positions of 30 and 60 bar being smaller than the 300 μm distance between the target spool positions of 5 and 30 bar, as shown in Fig. 15b. Moreover, it takes only 100 ms to achieve the pressure tracking for a drop step command from 60 to 5 bar, which occurs almost without an overshoot. Compared with a classic PID pressure controller (Ding et al., 2017; Liu et al., 2017), where the pressure adjustment time of the step response is typically 1 s or longer, the developed pressure FPID controller has clear advantages.

Therefore, the backpressure response is sufficient for pressure control in the designed IMVCHS.

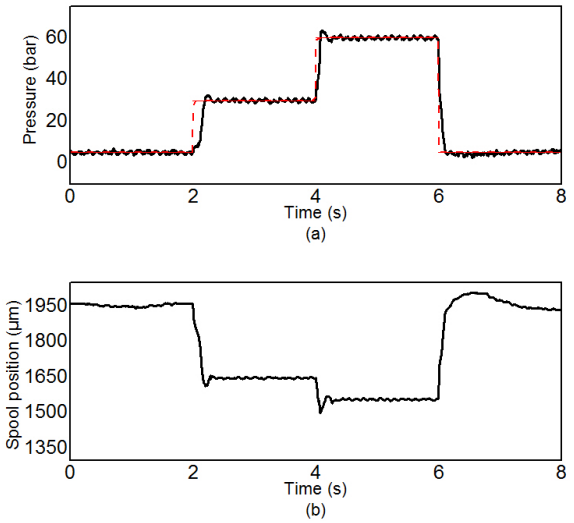

Fig. 15 Backpressure control performance: (a) backpressure; (b) spool position of valve 2

4.3 Experimental test on flow rate control

Experiments on the flow control characteristics are conducted to verify the control precision and response performance of the proposed flow controller. The output flow of the pump is set to 100 L/min, and the system pressure is set to 10 MPa. Valve 2 is driven using the position controller at a displacement of 2000 μm, and valve 1 is driven using the flow controller. The parameters of the flow FPID controller are set as: k_p=1.2, k_i=2.8, and k_d=14.0. The results of the inlet flow dynamic characteristic are given in Fig. 16a, and the corresponding chamber pressure performance and spool position are shown in Figs. 16b and 16c, respectively. Valve 1 starts with a spool position of −1533 μm, building to a flow rate of 30 L/min and chamber pressure of 14.4 bar. Based on the static measurement of a HYDROTECHNIK flow meter (QT100), the real flow rate varies from 29.6 to 30.6 L/min, which indicates the high control accuracy of the flow controller. The time for the flow to adjust from 30 to 70 L/min is 320 ms, and the overshoot is approximately 3%. When the spool position is stable at approximately −1810 μm, the inlet chamber pressure is maintained at 34.8 bar, and the flow rate is stable at 70 L/min. The flow error is controlled to within 2 L/min, which is mainly caused by the accuracy of the flow mapping and pressure oscillations, and the real flow tested by the flow meter ranges from 68.7 to 71.4 L/min. It takes only 250 ms to decrease the flow back to 30 L/min, and no overshoot occurs. This means that a fast response and accurate static characteristic are obtained using the proposed flow controller. Compared with a flow (velocity) controller (Xu et al., 2015; Ding et al., 2016, 2017; Cheng et al., 2017) whose flow (velocity) adjustment time of step response is also longer than 1 s, the developed flow FPID controller achieves a better performance in terms of the actuator speed control.

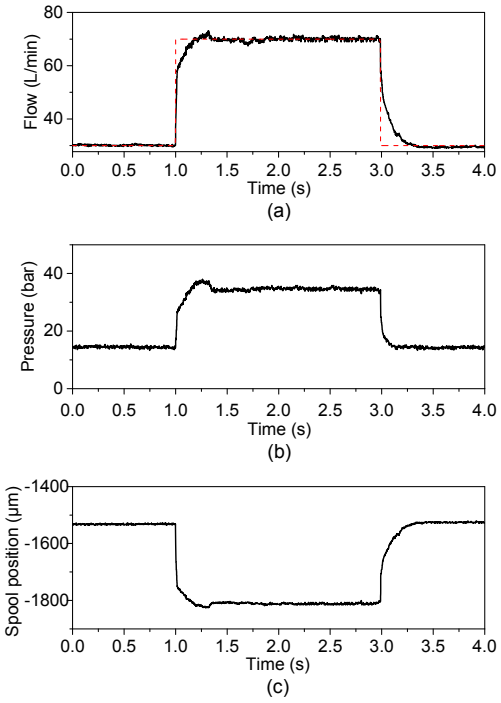

Fig. 16 Inlet flow control performance: (a) inlet flow; (b) pressure of inlet chamber; (c) spool position of valve 1

4.4 Experimental test on pressure and flow compound control

Pressure and flow compound controls are unique features of the IMVCHS, and can improve the actuator motion performance and reduce the energy consumption of the system. In this study, experiments on compound control are conducted. Valve 1 controls the flow rate of the inlet of the hydraulic bridge circuit,

and valve 2 controls the backpressure of the outlet chamber, which connects the hydraulic bridge circuit and tank. With a reference flow of 50 L/min, the performance of the backpressure step control is presented in Fig. 17. The results indicate that, using a fuzzy algorithm, the key control parameters of the two control loops are adaptively optimized, and therefore the backpressure change from 10 to 20 bar can be completed within 110 ms, as shown in Fig. 17b. Valves 1 and 2 move simultaneously to track the reference, valve 2 opens slightly to build a larger backpressure, and valve 1 opens more to match the increasing backpressure and maintain the flow rate, as shown in Fig. 17c. The distance between the stable valve 2 spool positions of 10 and 20 bar is approximately 270 μm. An overshoot of the backpressure is caused solely by a very small excess movement of valve 2. Because of the backpressure step, which finally affects the differential pressure through valve 1, a flow fluctuation of 2.2 L/min appears. The adjustment time for the flow rate is 170 ms, as shown in Fig. 17a.

The results of the backpressure step control from 20 to 30 bar are also compared. Owing to the closer distance of approximately 80 μm between the stable valve 2 spool positions of 20 and 30 bar, the backpressure adjustment time is reduced to 50 ms. However, an overshoot of 16% is caused by the synchronous increase in the opening area of valve 1, as shown in Fig. 17c, which results in a large flow peak, as shown in Fig. 17a, and also causes an overshoot of the backpressure.

Experiments on the flow step response under a constant backpressure were also conducted, the results of which are illustrated in Fig. 18. The backpressure is controlled at a constant value of 40 bar. The system starts with the target flow rate of 20 L/min, and valves 1 and 2 are stable at positions of −1533 and 1546 μm, respectively. When the flow controller tracks the 30 L/min reference, the flow adjusting time is 90 ms, and an overshoot is avoided, as shown in Fig. 18a. However, the step changes in the flow cause an instantaneous increase in the backpressure, as shown in Fig. 18b. At this moment, valve 2 increases the spool displacement, as shown in Fig. 18c, reducing the throttle loss and maintaining the backpressure at 40 bar. The adjustment time of the backpressure is 70 ms. Valves 1 and 2 remain at positions of −1624 and 1618 μm, respectively.

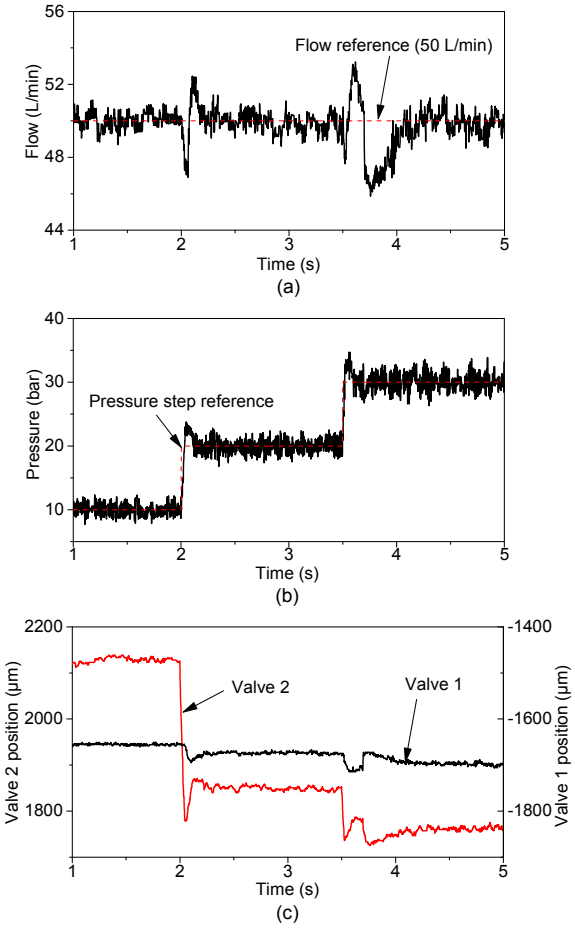

Fig. 17 Compound control performance under a constant flow rate: (a) inlet flow; (b) pressure of the outlet chamber; (c) spool positions

Similarly, the results of the flow rate step control from 30 to 40 L/min are also presented. The flow adjustment time remains at 90 ms, as shown in Fig. 18a, which is almost the same as the adjustment time of the flow step from 20 to 30 L/min. Because valve 1 operates within the linear working area, which means under the condition of a constant differential pressure, the spool moving distance required for each 10 L/min increment is basically the same, and is approximately 90 μm, as shown in Fig. 18c. It can be seen that the two flow step control experiments achieve the same dynamic response. Finally, valves 1 and 2 remain at positions of −1714 and 1700 μm,

respectively. Because valve 2 moves for a longer period of time under a flow step control of 30 to 40 L/min, the adjustment time of the backpressure increases to 100 ms.

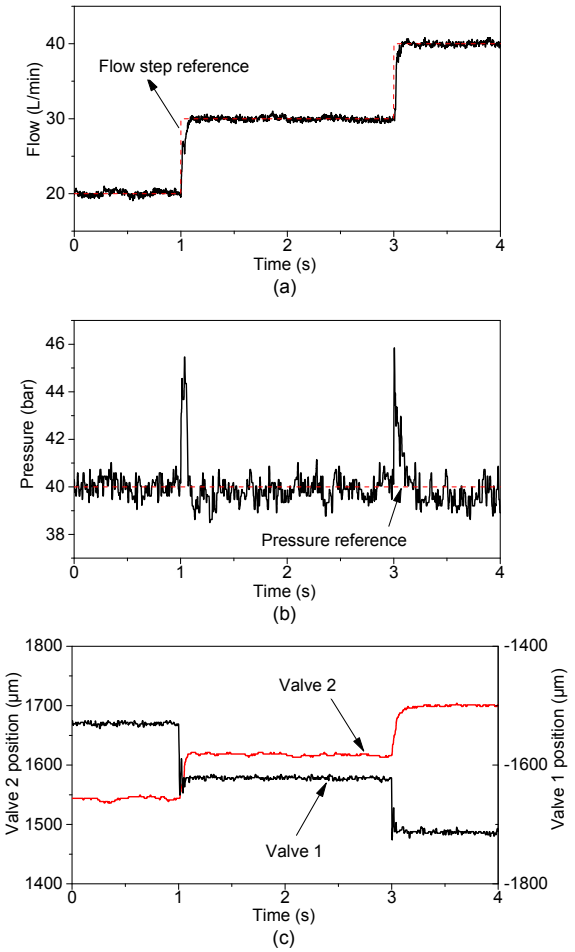

Fig. 18 Compound control performance under a constant backpressure: (a) inlet flow; (b) pressure of the outlet chamber; (c) spool positions

5 Conclusions

A programmable control system for an IMVCHS was proposed in this paper to realize pressure and flow compound control functions. A FPID control algorithm was applied to the spool position controller, and a two-level fuzzy closed-loop algorithm was adopted in both the pressure and flow controllers to achieve fast dynamics and stable statics. A feedback control algorithm for calculating the flow rate based on the pressure and spool position was employed to improve the flow rate control accuracy, the error of which can be controlled to within 2%. Experimental results demonstrated the effectiveness of the developed position, pressure, and flow controllers. The adjustment time of the spool position reaches 40 ms for 50% full strokes. The pressure adjustment time for 30 bar step control (backpressure of 30 to 60 bar) reaches 180 ms. The flow adjustment time for a 40 L/min step control (flow rate of 30–70 L/min) reaches 320 ms. The pressure and flow compound adjustment times are generally less than 200 ms, occasionally reaching less than 100 ms. The compound control experiments indicate that the proposed control system improves the response speed, control accuracy, and robustness of the IMVCHS under disturbances. Therefore, the IMVCHS can widen the real applications of independent metering control technology.

References

Acuña-Bravo W, Canuto E, Agostani M, et al., 2017. Proportional electro-hydraulic valves: an embedded model control solution. *Control Engineering Practice*, 62:22-35. https://doi.org/10.1016/j.conengprac.2017.01.013

Book R, Goering C, 2001. Mimo adaptive control of a “smart” hydraulic system. *International Journal of Smart Engineering System Design*, 3:15-28.

Borghi M, Zardin B, Pintore F, et al., 2014. Energy savings in the hydraulic circuit of agricultural tractors. *Energy Procedia*, 45:352-361. https://doi.org/10.1016/j.egypro.2014.01.038

Cheng M, Xu B, Zhang JH, et al., 2017. Pump-based compensation for dynamic improvement of the electrohydraulic flow matching system. *IEEE Transactions on Industrial Electronics*, 64(4):2903-2913. https://doi.org/10.1109/TIE.2016.2633478

Choi K, Seo J, Nam Y, et al., 2015. Energy-saving in excavators with application of independent metering valve. *Journal of Mechanical Science and Technology*, 29(1): 387-395. https://doi.org/10.1007/s12206-014-1245-5

Ding RQ, Xu B, Zhang JH, et al., 2016. Bumpless mode switch of independent metering fluid power system for mobile machinery. *Automation in Construction*, 68:52-64. https://doi.org/10.1016/j.autcon.2016.04.006

Ding RQ, Xu B, Zhang JH, et al., 2017. Self-tuning pressure-feedback control by pole placement for vibration reduction of excavator with independent metering fluid power system. *Mechanical Systems and Signal Processing*, 92: 86-106. https://doi.org/10.1016/j.ymssp.2017.01.012

Eriksson B, 2007. Control Strategy for Energy Efficient Fluid Power Actuators: Utilizing Individual Metering. PhD Thesis, Linköping University, Linköping, Sweden.

Eriksson B, Palmberg JO, 2011. Individual metering fluid power systems: challenges and opportunities. *Proceedings of the Institution of Mechanical Engineers, Part I: Journal of Systems and Control Engineering*, 225(2):196-211. https://doi.org/10.1243/09596518JSCE1111

Ge L, Quan L, Zhang XG, et al., 2017. Efficiency improvement and evaluation of electric hydraulic excavator with speed and displacement variable pump. *Energy Conversion and Management*, 150:62-71. https://doi.org/10.1016/j.enconman.2017.08.010

Hansen AH, Pedersen HC, Andersen TO, et al., 2011. Investigation of energy saving separate meter-in separate meter-out control strategies. Proceedings of the 12th Scandinavian International Conference on Fluid Power.

Hu H, Zhang Q, 2003. Multi-function realization using an integrated programmable E/H control valve. *Applied Engineering in Agriculture*, 19(3):283-290. https://doi.org/10.13031/2013.13660

Jansson A, Palmberg JO, 1990. Separate controls of meter-in and meter-out orifices in mobile hydraulic systems. *SAE Transactions*, 99(2):377-383.

Lantto B, Jansson A, Palmberg JO, 1989. A new concept of computer controlled electrohydraulic system: the p-q pump and valve control. Proceedings of the 2nd Bath International Fluid Power Workshop, p.99-114.

Linjama M, Vilenius M, 2005. Energy-efficient motion control of a digital hydraulic joint actuator. Proceedings of the 6th JFPS International Symposium on Fluid Power, p.640-645.

Linjama M, Paloniitty M, Tiainen L, et al., 2015. Mechatronic design of digital hydraulic micro valve package. *Procedia Engineering*, 106:97-107. https://doi.org/10.1016/j.proeng.2015.06.013

Liu B, Quan L, Ge L, 2017. Research on the performance of hydraulic excavator boom based pressure and flow accordance control with independent metering circuit. *Proceedings of the Institution of Mechanical Engineers, Part E: Journal of Process Mechanical Engineering*, 231(5):901-913. https://doi.org/10.1177/0954408916673117

Liu KL, Gao YJ, Tu ZH, et al., 2016. Energy-saving analysis of the independent metering system with pressure compensation for excavator's manipulator. *Proceedings of the Institution of Mechanical Engineers, Part I: Journal of Systems and Control Engineering*, 230(9):905-920. https://doi.org/10.1177/0959651816658191

Liu S, Yao B, 2002. Energy-saving Control of Single-rod Hydraulic Cylinders with Programmable Valves and Improved Working Mode Selection. SAE Technical Paper 2002-01-1343, Purdue University, West Lafayette, USA.

Liu S, Yao B, 2008. Coordinate control of energy saving programmable valves. *IEEE Transactions on Control Systems Technology*, 16(1):34-45. https://doi.org/10.1109/TCST.2007.903073

Opdenbosch P, Sadegh N, Book W, et al., 2011. Autocalibration based control for independent metering of hydraulic actuators. Proceedings of 2011 IEEE International Conference on Robotics and Automation, p.153-158. https://doi.org/10.1109/ICRA.2011.5980472

Plummer AR, Vaughan ND, 1996. Robust adaptive control for hydraulic servosystems. *Journal of Dynamic Systems, Measurement, and Control*, 118(2):237-244. https://doi.org/10.1115/1.2802309

Sitte A, Weber J, 2013. Structural design of independent metering control systems. Proceedings of the 13th Scandinavian International Conference on Fluid Power, p.261-270.

Sitte A, Beck B, Weber J, 2014. Design of independent metering control systems. Proceedings of the 9th International Fluid Power Conference.

Wei JH, Zhang Q, Li MJ, et al., 2016. High-performance motion control of the hydraulic press based on an extended fuzzy disturbance observer. *Proceedings of the Institution of Mechanical Engineers, Part I: Journal of Systems and Control Engineering*, 230(9):1044-1061. https://doi.org/10.1177/0959651816662562

Wu S, Jiao ZX, Yan L, et al., 2014. Development of a direct-drive servo valve with high-frequency voice coil motor and advanced digital controller. *IEEE/ASME Transactions on Mechatronics*, 19(3):932-942. https://doi.org/10.1109/TMECH.2013.2264218

Xu B, Ding RQ, Zhang JH, et al., 2015. Pump/valves coordinate control of the independent metering system for mobile machinery. *Automation in Construction*, 57:98-111. https://doi.org/10.1016/j.autcon.2015.04.012

Yao B, DeBoer C, 2002. Energy-saving adaptive robust motion control of single-rod hydraulic cylinders with programmable valves. Proceedings of 2002 American Control Conference, p.4819-4824. https://doi.org/10.1109/ACC.2002.1025421

Yao B, Liu S, 2002. Energy-saving control of hydraulic systems with novel programmable valves. Proceedings of the 4th World Congress on Intelligent Control and Automation, p.3219-3223. https://doi.org/10.1109/WCICA.2002.1020129

Yao J, Wang P, Cao XM, et al., 2018. Independent volume-in and volume-out control of an open circuit pump-controlled asymmetric cylinder system. *Journal of Zhejiang University-SCIENCE A (Applied Physics & Engineering)*, 19(3):203-210. https://doi.org/10.1631/jzus.A1600780

Yuan QH, Lew JY, 2005. Modeling and control of two stage twin spool servo-valve for energy-saving. Proceedings of 2005 American Control Conference, p.4363-4368.

https://doi.org/10.1109/ACC.2005.1470666

Zhang JH, Wang D, Xu B, et al., 2018. Experimental and numerical investigation of flow forces in a seat valve using a damping sleeve with orifices. *Journal of Zhejiang University-SCIENCE A (Applied Physics & Engineering)*, 19(6):417-430. https://doi.org/10.1631/jzus.A1700164

Zhong Q, Zhang B, Niu MJ, et al., 2017. Research on dynamic performance of independent metering control system. Proceedings of ASME/BATH 2017 Symposium on Fluid Power and Motion Control, p.V001T01A006. https://doi.org/10.1115/FPMC2017-4221

中文概要

题　目：基于两级模糊控制器的独立负载液压系统的压力流量复合控制特性研究

目　的：常规负载口独立控制研究多采用商业阀进行，因其阀芯位移控制器为封闭式结构，所以阀芯位移的动态特性难以调整，进而影响了系统的压力和流量控制性能。本文旨在探讨负载口独立控制系统中阀芯位移特性对系统压力和流量控制的影响，并研究提高系统压力和流量控制性能的方法。

创新点：1. 设计基于两级模糊比例积分微分（PID）的压力和流量控制器；2. 设计基于阀芯位移反馈的流量控制器；3. 建立试验模型，成功实现液压系统高动态压力流量复合控制。

方　法：1. 通过理论分析得到影响系统压力和流量的关键因素（公式（9）和（13））；2. 提出位移控制为内环、压力和流量控制为外环的两级模糊 PID 控制算法，并开发相应的控制系统（图 2~4）；3. 通过仿真和实验分析，验证本文提出的控制器所具有的阀芯位移、系统压力和流量的控制效果（图 13~18）。

结　论：1. 两级模糊 PID 控制器具有较好的系统压力和流量控制效果；2. 基于阀芯位移反馈的流量控制器具有较高的流量控制精度；3. 运用本文设计的可编程控制系统进行液压系统的压力流量复合控制，稳定时间小于 200 ms，使系统动态特性得到提高。

关键词：独立负载系统；压力流量复合控制；计算流量反馈；模糊 PID；两级闭环控制